

Remnant Fermi Surfaces in Photoemission

C. Kusko* and R.S. Markiewicz

Physics Department and Barnett Institute, Northeastern U., Boston MA 02115

Recent experiments have introduced a new concept for analyzing the photoemission spectra of correlated electrons – the remnant Fermi surface (rFs), which can be measured even in systems which lack a conventional Fermi surface. Here, we analyze the rFs in a number of interacting electron models, and find that the results fall into two classes. For systems with pairing instabilities, the rFs is an accurate replica of the true Fermi surface. In the presence of nesting instabilities, the rFs is a map of the resulting superlattice Brillouin zone. The results suggest that the gap in $\text{Ca}_2\text{CuO}_2\text{Cl}_2$ is of nesting origin.

Recently, a new experimental tool has been introduced [1] to parametrize photoemission (PE) data in strongly correlated metals: the ‘remnant Fermi surface’ (rFs). This is the locus of points in \vec{k} -space where the PE intensity associated with a particular quasiparticle peak falls to half of its peak value. For an ordinary metal, these points would correspond to the true Fermi surface, but in strongly correlated metals the points do not necessarily fall at the same energy – the rFs may display a considerable dispersion.

Ronning, et al. [1] measured the rFs of $\text{Ca}_2\text{CuO}_2\text{Cl}_2$ (CCOC), a half filled Mott insulator, and compared it with the rFs of optimally doped $\text{Bi}_2\text{Sr}_2\text{CaCu}_2\text{O}_8$ (BSCCO). When underdoped, the dispersion of BSCCO evolves toward that of CCOC [2]. Qualitatively, the rFs of CCOC seems consistent with Luttinger’s theorem, even though it displays a considerable dispersion. Despite this, the rFs’s of the two materials are strikingly different, and cannot evolve from each other via rigid band filling (they cross). A proper understanding of the rFs could lead to an improved model for the pseudogap in these materials.

In this Letter we analyze the rFs expected for a variety of interacting electron systems, and show that they do not necessarily provide information about the ‘true’ Fermi surface. The results fall into two classes, depending on whether the interaction can be characterized as ‘nesting’ or ‘pairing’. Only in the latter case is the rFs a reliable map of the Fermi surface. In the former case, it maps out the superlattice Brillouin zone generated by the nesting instability.

A number of different mechanisms have been proposed for the origin of pseudogaps in the cuprates. These include magnetic (spin density waves) [3], flux phase (RVB) [4–7], charge ordering (CDW) [6,8], and superconducting fluctuations [9]. These instabilities fall into two classes: nesting (the first three: associated with particle-hole propagators, and instabilities in the charge or spin susceptibilities at a nesting vector, here $\vec{Q} = (\pi, \pi)$) and

pairing (the last, associated with particle-particle propagators and the uniform susceptibility at $\vec{q} = 0$). In the cuprates, *all* of these instabilities may be analyzed within an $\text{SO}(6)$ group – the instability group of the Van Hove singularity [10]. We find that the rFs has two strikingly different origins in these two classes, but there is relatively little variation within a given class. In CCOC the rFs seems to indicate the locus of the reduced Brillouin zone, suggesting a nesting instability.

An important sum rule for ARPES that relates the integrated intensity to the momentum distribution has been introduced by Randeria et al. [11] and is given by

$$n(\vec{k}) = \int_{-\infty}^{\infty} d\omega f(\omega) A(\vec{k}, \omega), \quad (1)$$

where $A(\vec{k}, \omega)$ is the one particle spectral function of the model, $n(k) = \langle c_{\vec{k}}^\dagger c_{\vec{k}} \rangle$ is the momentum distribution and $f(\omega)$ is the Fermi function. Although $n(\vec{k})$ is a ground state property, they proved that in the limit of the sudden approximation the frequency integrated spectral function gives the momentum distribution. They employed this sum rule to determine the momentum distribution in BSCCO and YBCO. Ronning et al. [1] extended this methodology to strongly correlated electron compounds. By defining k_F as the point of steepest descent, they showed that even when strong Coulomb correlations destroy the Fermi-liquid character of the system, $n(\vec{k})$ still drops sharply, allowing the determination of a rFs.

In the following, we calculate the spectral function $A(\vec{k}, \omega)$ and the momentum distribution for mean field models with a variety of instabilities. Figure 1 illustrates the rFs’s associated with several nesting instabilities. The energy dispersion has the standard one-band form

$$e_{\vec{k}} = -2t_0(\cos k_x a + \cos k_y a) - 4t_1 \cos k_x a \cos k_y a, \quad (2)$$

with $t_0 = 0.25eV$, $t_1 = -0.45t_0$. The calculations follow those in Ref. [12] for CDW and s-wave superconductivity. The rFs’s for all the nesting instabilities are essentially identical: over part of the surface, there is no gap, and the rFs is dispersionless, coinciding with the true Fermi surface at $e_{\vec{k}} = E_F$; here $n(\vec{k}) = 1/2$ is mainly due to the Fermi function in Eq. 1. Over the rest of the zone, the rFs lies along the zone diagonals which determine the $\sqrt{2} \times \sqrt{2}$ nesting superlattice. On this part of the rFs there is considerable dispersion, and $n(\vec{k}) = 1/2$ due to the coherence factor, discussed below. By contrast, the

rFs for a pairing instability is always located below E_F at the superconducting gap, dispersionless for s-wave, dispersive for d-wave, but in both cases faithfully following the contours of the true Fermi surface.

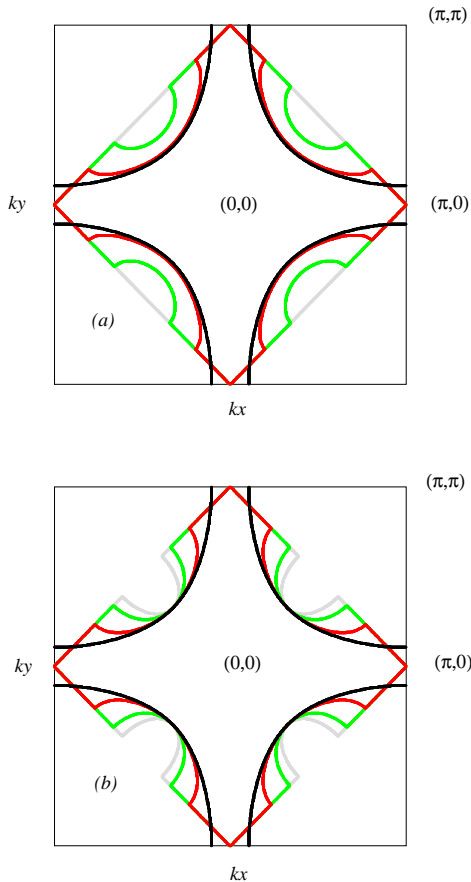


FIG. 1. Remnant Fermi surfaces for different nesting instabilities at $T=0K$. (a) evolution of the rFs toward a perfect square with increasing CDW gap; (from darkest to lightest) $O_{CDW}=0, 100, 300, 500$ meV. (b) the same evolution for a flux phase instability. Superconducting instabilities are not shown, since in this figure the rFs would coincide with the true Fermi surface.

If the pseudogap is due to a nesting instability competing with superconductivity, then there should be a characteristic evolution of the rFs with doping, from nesting-like at half filling to pairing-like in the overdoped regime. The phase diagram has been worked out for such a competition, both for CDW-to-s-wave superconductivity [12] and for flux phase to d-wave [7]. In both cases, we find the evolution of the rFs's is nearly identical. Figure 2 illustrates this evolution for the latter case. Note that since the phase at half filling is fully gapped (a Mott insulator), the rFs is perfectly square. The two limiting cases, insulator and optimally doped, bear a marked resemblance to the experimental observations [1].

In the calculations of Fig. 2, we took the competing phases to be d-wave superconductivity, with gap $\Delta_{\vec{k}}^d = \Delta^d \gamma_{\vec{k}}$, with $\gamma_{\vec{k}} = \cos k_x a - \cos k_y a$ and an or-

bital antiferromagnet [13,10], a nesting instability with gap $O_{\vec{k}}^{JC} = O^{JC} \gamma_{\vec{k}}$, which is an RVB state having a d-wave symmetry corresponding to a particle-hole excitation, essentially equivalent to the flux phase instability introduced by Affleck and Marston [14]. We consider a one-band model, Eq. 2, with correlation effects simulated by a doping dependent $t_0 = x t_0^*$, $t_0^* = 2.3eV$, and

$$t_1/t_0 = -0.52 \tanh(2.4x), \quad (3)$$

to pin the Van Hove singularity (VHS) close to the Fermi level over an extended range of doping [6,12]. We start with the following mean-field hamiltonian,

$$H = \sum_{\vec{k}, \sigma} \epsilon_{\vec{k}} c_{\vec{k}\sigma}^\dagger c_{\vec{k}\sigma} + O_{\vec{k}}^{JC} (c_{\vec{k}\sigma}^\dagger c_{\vec{k}+\vec{Q}\sigma} + h.c.) + \sum_{\vec{k}} \Delta_{\vec{k}}^d (c_{\vec{k}\uparrow}^\dagger c_{-\vec{k}\downarrow}^\dagger + h.c.). \quad (4)$$

with the quasiparticle dispersion given by,

$$E_{\pm, \vec{k}}^2 = \frac{1}{2} (\epsilon_{\vec{k}}^2 + \epsilon_{\vec{k}+\vec{Q}}^2 + 2\Delta_{\vec{k}}^2 + O_{\vec{k}}^{JC2} \pm \hat{E}_{\vec{k}}^2) \quad (5)$$

Performing a generalized Bogoliubov-Valatin transformation we find the following gap equations:

$$\Delta^d = U_{\Delta} \sum_{\vec{k}} \frac{\gamma_{\vec{k}}}{2} (\cos^2 \phi \sin 2\phi_+ \tanh \frac{\beta E_{+, \vec{k}}}{2} + \sin^2 \phi \sin 2\phi_- \tanh \frac{\beta E_{-, \vec{k}}}{2}) \quad (6)$$

and

$$O^{JC} = U_{O^{JC}} \sum_{\vec{k}} \frac{\gamma_{\vec{k}}}{4} \sin 2\phi (\cos 2\phi_+ \tanh \frac{\beta E_{+, \vec{k}}}{2} + \cos 2\phi_- \tanh \frac{\beta E_{-, \vec{k}}}{2}) \quad (7)$$

with $\hat{E}_{\vec{k}} = \sqrt{(\epsilon_{\vec{k}} - \epsilon_{\vec{k}+\vec{Q}})^2 + 4O_{\vec{k}}^{JC2}}$ and the angles defined by $\tan 2\phi_{\pm} = 2\Delta_{\vec{k}} / (\epsilon_{\vec{k}} + \epsilon_{\vec{k}+\vec{Q}} \pm \hat{E}_{\vec{k}})$,

$$\cos 2\phi = \frac{\epsilon_{\vec{k}} - \epsilon_{\vec{k}+\vec{Q}}}{\hat{E}_{\vec{k}}}, \quad (8)$$

and $\epsilon_{\vec{k}} = e_{\vec{k}} - E_F$. Solving the gap equations self-consistently with the coupling constants $U_{O^{JC}}=176$ meV and $U_{\Delta}=88$ meV, we find that the experimental phase diagram can be fit semi-quantitatively by this model (insert in Fig. 2) [15]. This phase diagram differs from that found in Ref. [12], but not because different instabilities were assumed. The main difference arises from the gap cutoffs: in Ref. [12], a phononic interaction was assumed, with cutoff $\hbar\omega = 45meV$; here, the interaction is taken as electronic, with no cutoff. This makes a significant difference in the phase boundary near half filling.

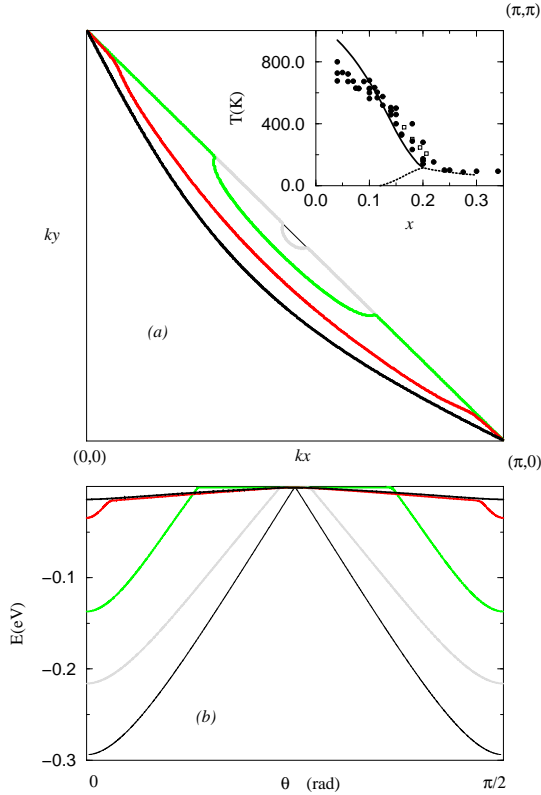


FIG. 2. (a) Evolution of the rFs from half filling to optimal doping at $T = 0K$ with self-consistent gap parameters for a model with d-wave superconductivity and flux phase. Curves from lightest to darkest: $x=0$ (thin line), 0.04, 0.1, 0.19 and 0.26 (black line). Inset: Pseudogap phase diagram for LSCO (filled circles) and YBCO (open squares) determined from transport [15]. Solid line - O^{JC} transition T^* ; dotted line - superconductivity transition T_c . (b) quasiparticle dispersion along the rFs plotted in (a), $\tan \theta = k_x/k_y$

In the above calculations, the shape of the Fermi surface evolved with doping, to mimic the effect of Van Hove pinning [16,6]. However, the evolution of the rFs for a nesting gap is generically toward a square Fermi surface as the gap is increased, as illustrated in Fig.1. The rFs has two parts, a true (hole pocket) Fermi surface on the ungapped part of the rFs, and a segment of square on the gapped part. With increasing gap magnitude, the former feature shrinks and the latter grows, until the full Fermi surface is gapped and the rFs is square. Note that due to the d-wave symmetry the rFs for a flux phase instability is pinned at the true Fermi surface along the diagonal $(0,0) - (\pi, \pi)$, Fig.1b. The shrinking of the true Fermi surface is reminiscent of the evolution in BSCCO reported by Norman, et al. [17]. It should be noted that the rFs is not equivalent to the minimum gap locus introduced by Ding, et al. [18].

The origin of the rFs can be understood from these calculations. In the competing flux phase-d-wave model, $n(\vec{k})$ can be written as

$$n(\vec{k}) = \frac{1}{2} \left(1 - \cos^2 \phi \cos 2\phi_+ \tanh \frac{\beta E_{+, \vec{k}}}{2} - \sin^2 \phi \cos 2\phi_- \tanh \frac{\beta E_{-, \vec{k}}}{2} \right). \quad (9)$$

For a pure d-wave superconductivity model this becomes

$$n(\vec{k}) = \frac{1}{2} \left(1 - \frac{\epsilon_{\vec{k}}}{E_{\vec{k}}} \tanh \frac{\beta E_{\vec{k}}}{2} \right), \quad (10)$$

with $E_{\vec{k}} = \sqrt{\epsilon_{\vec{k}}^2 + \Delta_{\vec{k}}^2}$, showing that the rFs coincides with the true Fermi surface: $n(\vec{k})=1/2$ when $\epsilon_{\vec{k}} = 0$. For a pure nesting model $n(\vec{k})$ is given by

$$n(\vec{k}) = \frac{1}{2} \left(1 - \cos^2 \phi \tanh \frac{\beta E_{+, \vec{k}}^{nest}}{2} - \sin^2 \phi \tanh \frac{\beta E_{-, \vec{k}}^{nest}}{2} \right), \quad (11)$$

with $E_{\pm, \vec{k}}^{nest} = (\epsilon_{\vec{k}} + \epsilon_{\vec{k}+\vec{Q}} \pm \hat{E}_{\vec{k}})/2$. As $T \rightarrow 0$, the two tanh's go to 1 or -1, so $n(\vec{k}) = 1/2$ when $\cos^2 \phi - \sin^2 \phi = 0$, or, from Eq.[8], $\epsilon_{\vec{k}} = \epsilon_{\vec{k}+\vec{Q}}$. For the present model, this is the superlattice Brillouin zone boundary.

In the underdoped regime, as temperature is lowered the cuprates pass first into the pseudogap phase, at temperature T^* , then into a superconducting phase at T_c . In the present scenario, T^* would signal a transition to a nested phase with a gap (or pseudogap if realistic fluctuations are included [3,19]), leaving hole pockets behind. Below T_c , an additional, pairing gap opens at the hole pockets. However, a careful look at the rFs shows a more complicated evolution, Fig.3a: the shape of the hole pockets changes, with an accompanying transfer of spectral weight from the nesting to the pairing parts of the rFs. Note that in Fig.3a the rFs has the same locus in k-space as the true hole pocket Fermi surface above T_c , but from Fig.3b there is a dramatic shift in dispersion of this rFs as the superconductivity gap opens.

In comparing these results to experiment, the rFs of CCOC clearly displays the square shape expected for a predominantly nesting interaction. This is consistent with all of the pseudogap models noted above, except for preformed pairs. In fact, preformed pairs would still be a possibility, if strong correlation effects renormalized the (true) Fermi surface to square at half filling. Such renormalization has been proposed previously [16,20], and is incorporated in Eq. 3. However, in these theories, the renormalization leads to greatly enhanced nesting, and is less favorable for pairing. The most likely conclusion is that the pseudogap in the underdoped cuprates represents some nesting instability, which is fundamentally competing with superconductivity. Clearly, since the cuprates are quasi-two-dimensional, there should be prominent superconducting fluctuations above T_c , but they do not represent the dominant part of the pseudogap.

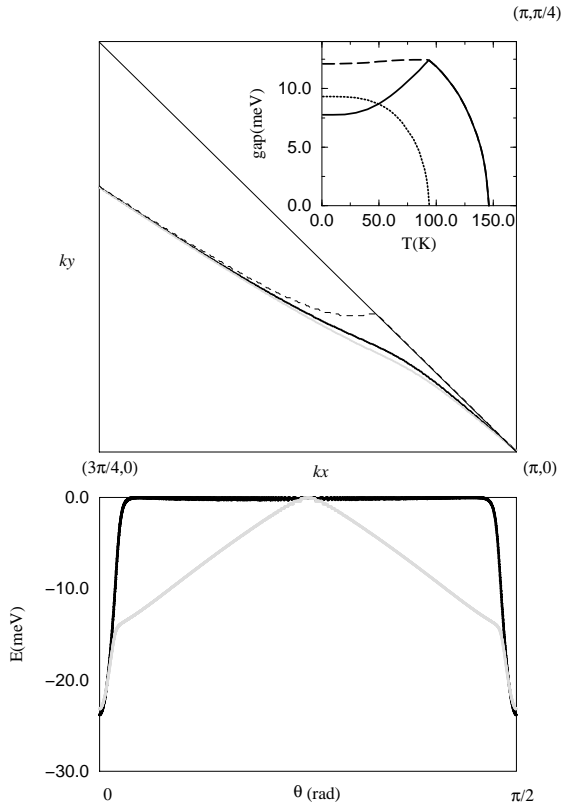


FIG. 3. (a) Evolution of the rFs with temperature for a fixed doping $x=0.19$: black line - $T=0\text{K}$, grey line - $T = T_c=94\text{K}$ ($\Delta^d=0$ meV), dashed line shows what the flux phase rFs at $T=0\text{K}$ would be if $\Delta^d=0$ meV. Inset: Temperature dependence of the superconducting and flux phase gaps; dotted line - Δ^d , solid line - O^{JC} , dashed line - $\sqrt{\Delta^d{}^2 + O^{JC}{}^2}$ (b) quasiparticle dispersion along the rFs plotted in (a).

The present results suggest a number of experimental tests. The rFs should be mapped out in the cuprates as a function of doping. In particular, the results of Norman, et al. [17] should be extended to the full rFs. Observation of a shift in spectral weight with temperature, Fig. 3 would provide strong evidence that the pseudogap is a nesting phenomenon, and not due to preformed pairs. Moreover, the rFs can be studied in other systems, to confirm the predicted properties. A start has already been made in CDW systems [22]. Mott insulators would be particularly of interest. It is believed that the insulating phase can form in the absence of magnetic order, hence without nesting. In the cuprates, there is a clear Néel transition, so a square rFs is not unexpected, but a study of rFs's in non-magnetic Mott insulators could prove most informative.

Publication 760 of the Barnett Institute.

*: On leave of absence from Institute of Atomic Physics, Bucharest, Romania.

- [1] F. Ronning, C. Kim, D.L. Feng, D.S. Marshall, A.G. Loesser, L.L. Miller, J.N. Eckstein, I. Bozovic, and Z.-X. Shen, *Science* **282**, 2067 (1998).
- [2] R.B. Laughlin, *Phys. Rev. Lett.* **79**, 1726 (1997).
- [3] A. Kampf and J. Schrieffer, *Phys. Rev.* **B41**, 6399 (1990), **B42**, 7967 (1990).
- [4] R.B. Laughlin, *J. Phys. Chem. Sol.* **56**, 1627 (1995).
- [5] X.-G. Wen and P.A. Lee, *Phys. Rev. Lett.* **76**, 503 (1996).
- [6] R.S. Markiewicz, *Phys. Rev.* **B56**, 9091 (1997).
- [7] E. Cappelluti and R. Zeyher, *Physica* **C312**, 313 (1999) and *Phys. Rev.* **B59**, 6475 (1999).
- [8] R.A. Klemm, unpublished.
- [9] V.J. Emery and S.A. Kivelson, *Nature* **374**, 434 (1995); M. Randeria, unpublished (cond-mat/9710223); Q. Chen, I. Kosztin, B. Jankó, and K. Levin, unpublished (cond-mat/9807414).
- [10] R.S. Markiewicz and M.T. Vaughn, *J. Phys. Chem. Sol.* **59**, 1737 (1998), and *Phys. Rev.* **B57**, 14052 (1998).
- [11] M. Randeria, H. Ding, J.C. Campuzano, A. Bellman, G. Jennings, T. Yokoya, T. Takahashi, H. Katayama-Yoshida, T. Mochiku, and K. Kadowaki, *Phys. Rev. Lett.* **74**, 4951 (1995).
- [12] R.S. Markiewicz, C. Kusko, and V. Kidambi, to be published, *Phys. Rev. B*, cond-mat/9807068.
- [13] H.J. Schulz, *Phys. Rev.* **B39**, 2940 (1989).
- [14] I. Affleck and J.B. Marston, *Phys. Rev.* **B37**, 3774 (1988).
- [15] B. Batlogg, H.Y. Hwang, H. Takagi, R.J. Cava, H.L. Kao and J. Kwo, *Physica* **235-240**, 130 (1994).
- [16] R.S. Markiewicz, *J. Phys. Cond. Matt.* **2**, 665 (1990).
- [17] M.R. Norman, H. Ding, M. Randeria, J.C. Campuzano, T. Yokoya, T. Takeuchi, T. Takahashi, T. Mochiku, K. Kadowaki, P. Guptasarma, and D.G. Hinks, *Nature* **392**, 158 (1998).
- [18] H. Ding, M.R. Norman, T. Yokoya, T. Takeuchi, M. Randeria, J.C. Campuzano, T. Takahashi, T. Mochiku, and K. Kadowaki, *Phys. Rev. Lett.* **78**, 2628 (1997).
- [19] R.S. Markiewicz, *Physica* **C169**, 63 (1990).
- [20] Earlier references summarized on p. 1223 of Ref [21];
- [21] R.S. Markiewicz, *J. Phys. Chem. Sol.* **58**, 1179 (1997); N. Furukawa and T.M. Rice, *J. Phys. Cond. Matt.* **10**, L381 (1998), and N. Furukawa, M. Salmhofer and T. M. Rice, unpublished (cond-mat/9806159); G. Hildebrand, E. Arrigoni, C. Gröber, and W. Hanke, unpublished (cond-mat/9801181).
- [22] Th. Pillo, J. Hayoz, H. Berger, M. Gioni, L. Schlapbach, and P. Aebi, cond-mat/9902327.